FAST FISSION YIELDS IN THE SYNTHESIS OF THE ^{296}Lv SUPERHEAVY ELEMENT AT E^*=30 MeV

D. ARANGHEL[1,2], A. SANDULESCU[1,3,4]

[1]"Horia Hulubei" National R&D Institute for Physics and Nuclear Engineering, Reactorului 30, RO-077125, POB-MG6, Măgurele-Bucharest, Romania
[2]Extreme Light Intrastructure Nuclear Physics (ELI-NP), Reactorului 30, RO-077125, POB-MG6, Magurele-Bucharest, Romania
[3]Geodynamic Institute of the Romanian Academy, 19-21 Jean Louis Calderon, R-020032, Bucharest 37, Romania
[4]Academia Romana, Calea Victoriei 125, Bucharest, Romania

Received March 23, 2015

The fragmentation potential for all mass asymmetries is evaluated at an excitation of 30 MeV. The isomeric minima observed for the adiabatic energy surface are still present but their wells are attenuated. The fast fission mass yield distributions were evaluated from these isomeric minima at 30 MeV excitation energy and are found consistent with experimental data.

Key words: Macroscopic-microscopic model, shell effects, isomer states, superheavy nuclei.

PACS: 21.60.Cs.

1. INTRODUCTION

The macroscopic-microscopic fragmentation potential based on the Woods-Saxon two-center shell model in a wide range of mass asymmetries revealed in the case of the superheavy nucleus ^{296}Lv the formation of several minima [1]. The potential in the configuration space spanned by five degrees of freedom is obtained by extrapolating the fusion trajectory with ^{48}Ca as projectile. It was considered that these minima are responsible for the quasifission structure distribution obtained experimentally [2, 3]. The compound nucleus is formed in the metastable states managed by the potential minima and decays by cold fission, reaching the ground state deformations of the fragments. The origin of these isomeric minima were investigated in Ref. [4]. The importance of the shell effects was emphasized for the existence of the isomeric minima. A problem remains questionable. The experimental data of Ref. [3] are reported for 33 MeV excitation energy. So, the behavior of the nucleus in this energy range should be also investigated. In the following, the fragmentation potential is calculated for the same value of the excitation energy by involving statistical arguments. In the frame of the model, the excitation energy determines mainly a modification of the shell and paring corrections. The emission of neutrons at scission [5] is neglected.

2. THEORETICAL FORMALISM

As mentioned, we computed the total energy of the nuclear system in the framework of the macroscopic-microscopic method. Within this approach, it is assumed that a macroscopic model, as the liquid drop one, describes quantitatively the smooth trends of the potential energy with respect to the particle number and deformation. The shell model is responsible for the local fluctuations. These local fluctuations are calculated with the Strutinsky prescriptions. The total energy of the nucleus $V(q)$ is

$$V(q) = V_{LDM}(q) + \delta V(q) \tag{1}$$

where $V_{LDM}(q)$ is the liquid drop energy and $\delta V(q)$ are the shell and pairing corrections. These energy values depend on a set of generalized coordinates q associated to the degrees of freedom of the nuclear shape parametrization. A condition of consistency must be fulfilled: the same shape must be used in computing the liquid drop energy and the shell effects. Different nuclear shape parametrizations are used in the literature [12–15]. In the following, a nuclear shape obtained by smoothly joining two spheroids of semi-axis a_i and b_i (i=1,2) with a neck surface generated by the rotation of a circle of radius R_3 around the axis of symmetry is used. This parametrization is characterized by five independent generalized coordinates $\{q_i\}$ (i=1,5). The degrees of freedom are the elongation R given by the distance between the centers of the spheroids; the necking parameter $C_3 = S/R_3$ related to the curvature of the neck, the eccentricities $\epsilon_i = \sqrt{1-(b_i/a_i)^2}$ (i=1,2) associated with the deformations of the nascent fragments and the mass asymmetry parameter $\eta = (A_1 - A_2)/(A_1 + A_2)$, where A_1 and A_2 are the mass numbers of the nascent fragments. These numbers are obtained by calculating the virtual volumes of the two ellipsoids with semi-axis a_i and b_i.

The macroscopic energy (liquid drop one) is obtained in the framework of the Yukawa-plus-exponential model [16] extended for binary systems with different charge densities as detailed in Ref. [17, 18]. The parameters of the model are taken from Ref. [19]. The macroscopic energy contains several terms: the surface energy, the Coulomb energy and its diffusivity, the volume energy, the Wigner term and the A_0-one. When the nucleus changes the deformation, the single particle levels are rearranged. As mentioned, the internal structure of the nucleus is translated in shell and pairing corrections within the Strutinsky prescriptions [14]. These corrections represent the varying parts of the total binding energy caused by the shell structure. The single-particle-level diagrams are computed within the Woods-Saxon superasymmetric two- center shell model [27]. The Woods-Saxon potential, the spin-orbit term and the electrostatic potential are diagonalized within the two-center semi-symmetric oscillator wave functions [20–23]. This parametrization was widely used by the Bucharest group in the calculations addressing the cluster and alpha decay

[24–31], the fission [32–38] and its dissipation, the pair breaking [39, 40], the generalization of time dependent pairing equations [27], the heavy element synthesis [41, 42], and the double beta decay [43]. Being able to treat extreme asymmetries of the fission process, the two center approach emerges as a competitive model for the alpha decay which is usually treated with preformation models [44–46].

It is worth to mention that the stability of the superheavy nuclei was predicted within the macroscopic-microscopic approximation [6]. Therefore the model is reliable. Latter on, the optimum choice of the two partners that collide to form a superheavy nucleus was determined in the framework of the fragmentation theory [7] by considering the fusion as a cold rearrangement process. Investigating the total potential energy, it was predicted that the most favorable reactions are connected with the valley of the Pb [8–10]. An analogue most favorable valley was found for cluster decay [11]. In Ref. [9], the ^{48}Ca was proposed as a projectile on various transuranium targets.

The shell effects can be considered to be dependent on the excitation energy of the nucleus [47]. If we use the semi-empirical relation [48]:

$$E^* = \frac{1}{9} A\theta^2 - \theta \tag{2}$$

then, a dependence between the excitation energy E^* and the square of the temperature θ is postulated [49]. This dependence can be parametrized as follows:

$$V = V_{LDM} + \delta V \exp(-\theta^2/\theta_0^2) \tag{3}$$

where θ_0=1.5 MeV.

3. RESULTS

The path in the multidimensional configuration was used for the family of nuclear shapes that begins from the ground state and reach the scission point, as described in Ref. [1]. A trajectory was deduced for the ^{48}Ca+^{248}Cm system and was extrapolated for all the other mass asymmetries. For this purpose the eccentricities of the ground states were computed for all partners in the reaction ^{A_1}Z$_1$+^{A_2}Z$_2$=^{296}116.

In the Fig. 1, the energy surface for the fragmentation potential at an excitation energy of 30 MeV is displayed as function of the mass asymmetry $\eta = (A_1 - A_2)/(A_1 + A_2)$ and the elongation R coordinates. It is important to note that also the spherical ground state energy value of the compound nucleus increased with approximately 2.5 MeV due to the variation of the shell effects. The spherical shape corresponds to the asymmetry $\eta = 0$ and the elongation R=0 fm. When the distance between the nascent fragments increases, the two nuclei reach their individualities, and after the scission their final eccentricities. In the upper panel of Fig. 1 we represented the potential from symmetric fission up to alpha emission as a surface. In the

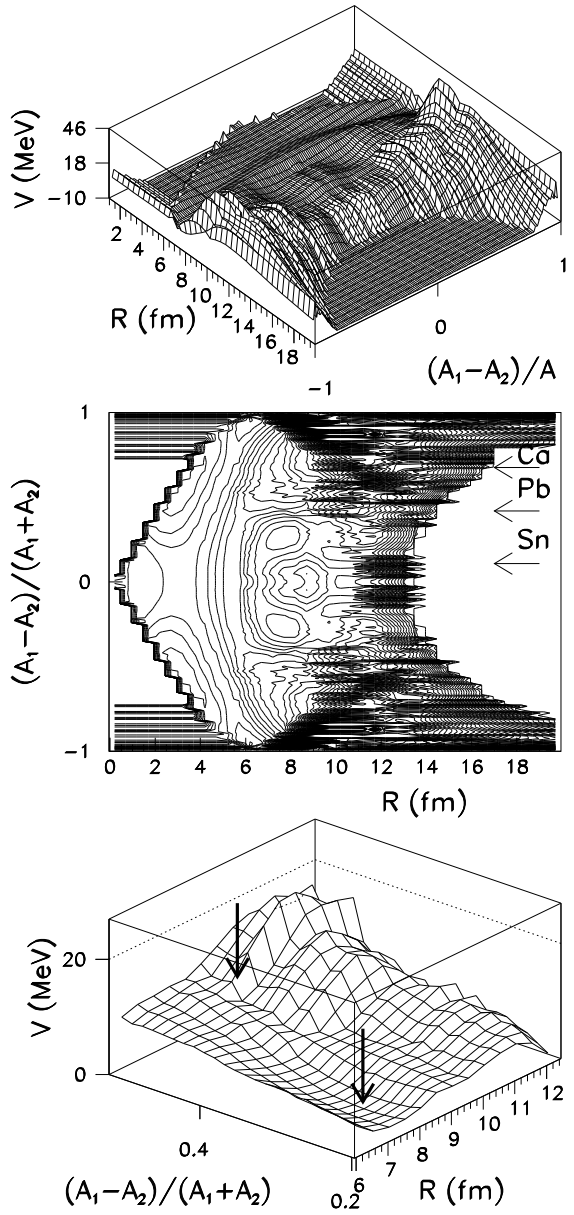

Fig. 1 – Potential energy surface as function of the mass asymmetry $(A_1 - A_2)/(A_1 + A_2)$ and of the elongation R at the excitation energy E^*=30 MeV. In the lower panel, the two minima are identified with arrows.

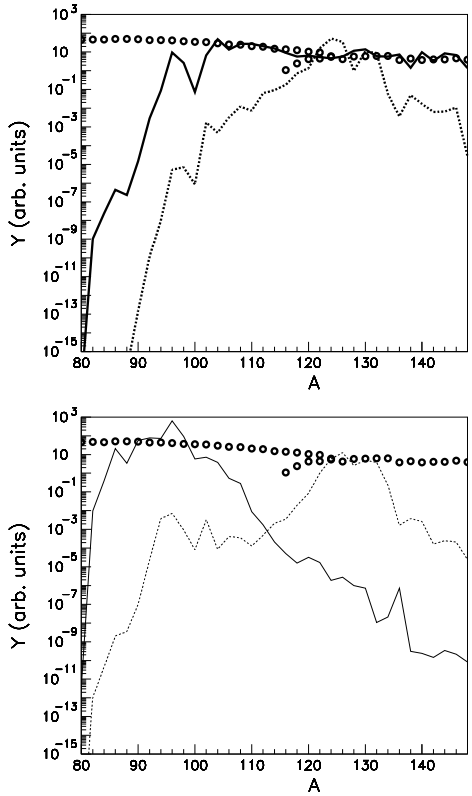

Fig. 2 – The yields obtained from the two isomeric minima as function of the light fragment mass. The full line is for the second isomeric well while the dashed line is for the first one. The upper panel refers to a dissipated energy of 30 MeV while the lower one is for zero excitation energy. The experimental data are marked with circles.

middle panel, the same potential is represented as equipotential lines. In the lower panel, only a detail of the deformation energy surface is displayed in order to identify the two isomer minima. One of them is located at R=7.5 fm and η=0.24. At zero excitation energy this minimum is located at R=7.4 fm and η=0.27. The second minimum is located at R=8.7 and η=0.44. At zero excitation energy, this minimum is located at R=8.6 fm and η=0.48. From these two minima we constructed fission trajectories that arrive in the touching configurations for all mass asymmetries like a fan. We computed the action integral for each fission path. The Gamow factors obtained from these action integrals are inversely proportional with the theoretical yields. Moreover, the action integral along the paths that connect the minima and the exit point of the barrier for the ^{48}Ca+^{248}Cm systems was also computed. These action integral values supply the knowledge of the compound nucleus formation prob-

abilities in both isomeric states. Finally, we multiplied the probability to obtain a compound nucleus in one of the isomeric state with the theoretical yield probabilities of all possible partitions to obtain the total yield distribution. The later takes into consideration the formation of the compound nucleus with ^{48}Ca projectile. We obtained two theoretical yield distributions, one for each isomeric state. These two distributions are plotted in the upper panel of Fig. 2. For the yield distribution that pertains to the first isomeric state, a dashed line is used. The theoretical curves succeed to reproduce the main behavior of the experimental data plotted with circles. If we compare the distributions of Fig. 2 with those obtained at zero excitation energy given in the lower panel, we can remarks two main differences. The actual distributions are spread over the mass numbers and the difference between their maximal values is lower. Moreover, maximal values of the excited mass distributions are shifted to lower mass asymmetry. So, we can predict that quasifission products are shifted towards symmetric partitions when the excitation energy increase. Our mass distribution is calculated by assuming that all the energy brought by the projectile are transformed in intrinsic excitations. In reality, the available energy can be stored partially as collective kinetic energy. Therefore, the experimental distribution should be a convolution of distributions calculated at different excitation energies. At low excitation energies, the peak for the distribution obtained at $A_2 \approx 90$ dominates. In this picture, the theory explains the existence of two different quasifission distributions obtained in the fusion ^{48}Ca+^{248}Cf. If we consider that the quasi-fission process is made without dissipation, the maximum yield is obtained when ^{96}Sr+^{200}Pt=^{296}Lv. So, if the two partners are detected experimentally in the same time, we can conclude that an isomeric state of the superheavy element ^{296}Lv is obtained.

In conclusion, the mass distributions for fast fission produced during the synthesis of superheavy elements are due to minima in the potential energy. These minima are due to shell effects and are persistent up to dissipated energy that amounts to several tens of MeV.

Acknowledgements. We thank to M. Mirea for providing us the two center Woods-Saxon codes. Work supported by CNCS - UEFISCDI, project number PN - II - ID - PCE - 2011 -3 - 0068.

REFERENCES

1. A. Sandulescu and M. Mirea, Eur. Phys. J. A **50**, 110 (2014).
2. R. Budaca, A. Sandulescu, and M. Mirea, Mod. Phys. Lett. A **30**, 1550129 (2015).
3. M.G. Itkis, A.A. Bogachev, I.M. Itkis, G.N. Knyazheva, N.A. Kondratiev, E.M. Kozulin, L. Krupa, Yu.Ts. Oganessian, I.V. Pokrovsky, E.V. Prokhorova, A.Ya. Rusanov, V.M. Voskresenski, V.A. Rubchenya, and W.H. Trzaska, Int. J. Mod. Phys. E **16**, 957 (2007).

4. D. Aranghel and A. Sandulescu, Rom. J. Phys. **60**, 147 (2015).
5. M. Rizea and N. Carjan, Proc. Rom. Acad. Series A **16**, 176 (2015).
6. A. Sobiczewski and K. Pomorski, Prog. Part. Nucl. Phys. **58**, 292 (2007).
7. A. Sandulescu, R.K. Gupta, W. Scheid, and W. Greiner, Phys. Lett. B **60**, 225 (1976).
8. R.K. Gupta, C. Parvulescu, A. Sandulescu and W. Greiner, Z. Phys. A **283**, 217 (1977).
9. R.K. Gupta, A. Sandulescu, and W. Greiner, Phys. Lett. B **67**, 257 (1977).
10. R.K. Gupta, A. Sandulescu, and W. Greiner, Z. Naturforsch **32a**, 704 (1977).
11. A. Sandulescu, D.N. Poenaru, and W. Greiner, Sov. J. Part. Nucl. **11**, 528 (1980).
12. J.R. Nix, Ann. Rev. Nucl. Sci. **22**, 65 (1972).
13. W.J. Swiatecki and S. Bjornholm, Phys. Rep. **4**, 325 (1972).
14. M. Brack, J. Damgaard, A.S. Jensen, H.C. Pauli, V.M. Strutinsky, and C.Y. Wong, Rev. Mod. Phys. **44**, 320 (1972).
15. V.Yu. Denisov, Phys. Rev. C **91**, 024603 (2015).
16. K.T.R. Davies and J.R. Nix, Phys. Rev. C **14**, 1977 (1976).
17. M. Mirea, O. Bajeat, F. Clapier, F. Ibrahim, A.C. Mueller, N. Pauwels, and J. Proust, Eur. Phys. J. A **11**, 59 (2001).
18. D.N. Poenaru, M. Ivascu, and D. Mazilu, Comput. Phys. Commun. **19**, 205 (1980).
19. P. Moller, J.R. Nix, W.D. Myers, and W.J. Swiatecki, Atom. Data Nucl. Data Tabl. **59**, 185 (1995).
20. E. Badralexe, M. Rizea, and A. Sandulescu, Rev. Roum. Phys. **19**, 63 (1974).
21. M. Mirea, Phys. Rev. C **54**, 302 (1996).
22. M. Mirea, Nucl. Phys. A **780**, 13 (2006).
23. J. Maruhn and W. Greiner, Z. Phys. **251**, 431 (1972).
24. A. Sandulescu, M. Mirea, and D.S. Delion, EPL **101**, 62001 (2013).
25. M. Mirea, Rom. J. Phys. **60**, 156 (2015).
26. M. Mirea, Phys. Rev. C **63**, 034603 (2001).
27. M. Mirea, Phys. Rev. C **78**, 044618 (2008).
28. M. Mirea, A. Sandulescu, and D.S. Delion, Nucl. Phys. A **870-871**, 23 (2011).
29. M. Mirea, A. Sandulescu, and D.S. Delion, Eur. Phys. J. A **48**, 86 (2012).
30. A. Sandulescu and M. Mirea, Rom. Rep. Phys. **65**, 688 (2013).
31. M. Mirea, Eur. Phys. J. A **4**, 335 (1999).
32. M. Mirea, Phys. Rev. C **83**, 054608 (2011).
33. M. Mirea, Phys. Lett. B **717**, 252 (2012).
34. M. Mirea, D.S. Delion, and A. Sandulescu, Phys. Rev. C **81**, 044317 (2010).
35. A.-M. Micu and M. Mirea, Rom. J. Phys. **58**, 939 (2013).
36. N.S. Shakib, M.F. Rahimi, and M.M. Firoozabadi, Rom. Rep. Phys. **65**, 401 (2013).
37. M. Mirea and R.C. Bobulescu, J. Phys. G. **37**, 055106 (2010).
38. M. Mirea, L. Tassan-Got, C. Stephan, C.O. Bacri, and R.C. Bobulescu, Europhys. Lett. **73**, 705 (2006).
39. M. Mirea, Phys. Lett. B **680**, 316 (2009).
40. M. Mirea, Phys. Rev. C **89**, 034623 (2014).
41. M. Mirea, D. S. Delion, and A. Sandulescu, EPL **85**, 12001 (2009).
42. A. Sandulescu and M. Mirea, Rom. J. Phys. **58**, 1148 (2013).
43. T.E. Pahomi, A. Neacsu, M. Mirea, and S. Stoica, Rom. Rep. Phys. **66**, 370 (2014).
44. I. Silisteanu and A.I. Budaca, Rom. J. Phys. **58**, 1198 (2013).
45. I. Silisteanu and A.I. Budaca, Rom. Rep. Phys. **65**, 757 (2013)

46. D.S. Delion, R.J. Liotta, and R Wyss, Phys. Rev. C **76**, 044301 (2007).
47. A.S. Jensen and J. Damgaard, Nucl. Phys. A **203**, 578 (1973).
48. R.K. Gupta and W. Greiner, in Heavy Elements and Related New Phenomena, Eds. W. Greiner and R.K. Gupta, chapter 14, World Scientific, 1999.
49. K.J. Le Couteur and D.W. Lang, Nucl. Phys. **13**, 32 (1959).